ECASIA special issue paper

SURFACE and INTERFACE ANALYSIS

Received: 1 September 2015 Revised: 15 February 2016 Accepted: 15 February 2016 Published online in Wiley Online Library

(wileyonlinelibrary.com) DOI 10.1002/sia.5992

Chemistry and electronics of single layer MoS_2 domains from photoelectron spectromicroscopy using laboratory excitation sources

M. Frégnaux,[a,b] H. Kim,[a,b] D. Rouchon,[a,b] V. Derycke,[c] J. Bleuse,[d,e] D. Voiry,[f] M. Chhowalla[f] and O. Renault[a,b]*

In the recent context of emerging two-dimensional (2D) materials, a comprehensive set of spatially resolved photoelectron spectroscopic techniques providing information ranging from surface chemical states to electronic band structure must be available at the practical level (i.e. from laboratory-based instrumentation) for a better understanding of their outstanding properties. We highlight recent capabilities of X-ray PhotoElectron Emission Microscopy (XPEEM) and reciprocal-space VUV-PEEM (*k*PEEM) for addressing this issue, with a report on microscopic analyses of chemical vapor deposited (CVD) molybdenum disulfide (MoS_2) domains. These include band structure imaging with event-counting detection allowing to perform angle-resolved ultra-violet photoelectron spectroscopy (ARUPS) in a parallel way with energy resolution of 200 meV and less, and *k* resolution of 0.05 $Å^{-1}$.

Keywords: 2D materials; transition metal dichalcogenides; XPEEM; work function; electronic band structure

Introduction

Two-dimensional transition metal dichalcogenides (2D-TMDs), such as MoS_2, have recently gained increasing attention because of the combination of their unique optoelectronic properties with their atomically thin character. MoS_2 monolayer (1L) consists of a single layer of Mo atoms sandwiched between two layers of S atoms in a trigonal prismatic structure [1]. Easily obtained by exfoliation or chemical vapor deposition (CVD), few micrometer MoS_2 domains have a remarkable direct band gap of 1.9 eV in the 1L regime. Indeed, this indirect-to-direct band gap transition originates from the missing interlayer interaction in 1L form [2] and the strong spin orbit coupling induced split valence bands (~160 meV^3) because of broken inversion symmetry. These properties make 2D materials of great interest for nano-electronic devices [4] or spintronics applications.

In this context, advanced highly resolved XPS imaging methods, also able to provide a comprehensive set of information, are needed. X-ray PhotoElectron Emission Microscopy (XPEEM) [5–7] is a powerful tool to study 2D-TMDs [8] because it provides access to spectroscopic information with high-energy (<0.5 eV), lateral (<0.5 μm to 1 μm in routine analysis [9,10]) and wave-vector (<0.1 $Å^{-1}$) resolutions. XPEEM therefore goes far beyond the capabilities of current XPS microscopes because very high lateral resolutions in core-level imaging are reached and complementary work function mapping and valence band structure imaging can be performed. The highly resolved (better than 150 nm) secondary electron PEEM images also enable easy identification of particular (e.g. defect-free) 2D-TMD domains (size ranging from few nm to few ten μm) in order to perform selectively various kinds of spectroscopic imaging (in the XPS, UPS and ARUPS regime) as well as quantitative, area-selected (micro-) spectroscopy. In the momentum, so-called *k*PEEM, microscopy mode (equivalent to microscopic ARUPS but with parallel angular detection), the technique can probe the valence band of individual 1L MoS_2 domain providing, after data treatment, significant information such as experimental hole effective mass values.

Here, we highlight recent capabilities of XPEEM and *k*PEEM for addressing the issue of spatially resolved photoemission for 2D materials, with an example of microscopic analyses on MoS_2 1L domains.

Experimental

This work was performed on MoS_2 1L produced by chemical vapor deposition (CVD) and transferred onto either gold (Au) substrate or silicon (Si) capped with 285-nm-thick oxide. More details on the MoS_2 growth can be found elsewhere [11]. The effective presence

* *Correspondence to: O. Renault, Univ. Grenoble Alpes, F-38000 Grenoble, France, CEA, LETI, MINATEC Campus, F-38054 Grenoble, France. E-mail: olivier.renault@cea.fr*

a *Univ. Grenoble Alpes, F-38000, Grenoble, France*

b *CEA, LETI, MINATEC Campus, F-38054, Grenoble, France*

c *CEA, IRAMIS, F-91191, Gif-sur-Yvette, France*

d *Univ. Grenoble Alpes, F-38000, Grenoble, France*

e *CEA, INAC, F-38054, Grenoble, France*

f *Materials Science and Engineering, Rutgers University, 607 Taylor Road, Piscataway, New Jersey 088854, USA*

of MoS_2 domains and their good crystallinity were first verified by atomic force microscopy (AFM) and Raman spectrometry. The thickness obtained from AFM measurements was found to be 0.81 nm and 0.83 nm for MoS_2 sheets transferred onto Au and Si substrate, respectively. These values are consistent with previous analyses on exfoliated 1L (0.65 nm) [4]. Raman analysis (spectra not shown here) clearly evidenced the presence of two peaks at 384.7 and 403.2 cm^{-1} corresponding, respectively, to the specific MoS_2 E^1_{2g} (out-of-plane) and A_{1g} (in-plane) vibrational modes. Their frequencies are shifted compared with bulk material (383 and 408 cm^{-1}, respectively) [12]. Indeed, the Raman response of 2D-TMDs is known to be thickness dependent and, here, the measured values correspond to those obtained on MoS_2 1L [12].

Combined XPEEM-*k*PEEM measurements were performed with a *NanoESCA* spectromicroscope (ScientaOmicron) [5,6] at room temperature and a base pressure of 5×10^{-11} mbar, and using different laboratory excitation sources impinging the sample at angle of ~22° with respect to the surface. The instrument was recently up-graded with a low noise, event-counting detection enhancing the sensitivity. Before XPEEM/*k*PEEM imaging, the samples were heated at 450 °C for 1 h in vacuum to remove adsorbates, as confirmed by a drastic decrease after annealing of the C 1s core-level peak in the XPS survey micro-spectrum.

For work-function mapping, secondary electron PEEM imaging was performed with a VUV He I cold cathode lamp ($h\nu = 21.2$ eV). For this, photoelectron image series across the photoemission threshold were acquired within a field of view of 114.9 μm and an energy range of $E\text{-}E_F = 2.0$ to 5.5 eV (0.05 eV energy steps and 3-s acquisition time per image).

Core-level spectroscopic imaging and XPS microspectroscopy were performed with a monochromated Al Kα X-ray source ($h\nu = 1486.7$ eV – 200 μm spot size). For microspectroscopy, the area of interest was defined within the 111-μm microscope field-of-view by closing the field aperture of the PEEM on the selected MoS_2 domain. For core-level imaging, the contrast aperture of 500 μm (i.e. angular aperture located in the back-focal plane and enhancing the lateral resolution up to 500 nm[9]) was used as a compromise between the effective lateral resolution and overall transmission of the microscope. In both cases, the analyzer pass energy of 100 eV and entrance slit size of 1 mm resulted in an overall energy resolution of 0.4 eV.

Finally, *k*PEEM data were collected using He I radiation within a field of view in reciprocal space of 5.2 $Å^{-1}$. In this setup, the area of interest on the sample surface is defined by the field aperture closed down to about 30 μm and located in the first intermediate image plane of the PEEM. A transfer lens projects the 1500-μm diameter disk of the focal plane (fully open contrast aperture) through the imaging spectrometer onto the detector providing a 2D k-space dimension of about 2.5 $Å^{-1}$ in radius, with a *k*-resolution of about 0.05 $Å^{-1}$. Electronic band structure measurements were carried out at room temperature in event-counting detection mode with an energy resolution of ~200 meV (similar to Ref. 17). Valence photoelectron image series in *k*-space were acquired within an energy range $E\text{–}E_F$ of 13.2 to 21.2 eV, with energy steps of 0.05 eV and acquisition times of 11 s per image. The final data was obtained by summing up 20 series after compensating for a slight energy drift from one series to the other because of residual time-dependent charging. Projections along high symmetry directions in the Brillouin zone (BZ) were used to generate band dispersion plots. For enhancement of image contrast and a better visualization of the band dispersions, a second derivative of the *k*PEEM intensity plot is presented.

Results and discussion

Figure 1 (a) shows an energy-filtered XPEEM image of a well-defined triangular CVD MoS_2 1L domain with a grain size of ~50 μm on Au substrate. Part (b) presents the corresponding work-function map over a larger field of view. The energy dependent intensity curve for each pixel in the image series was fitted using a complementary error function to obtain the local work

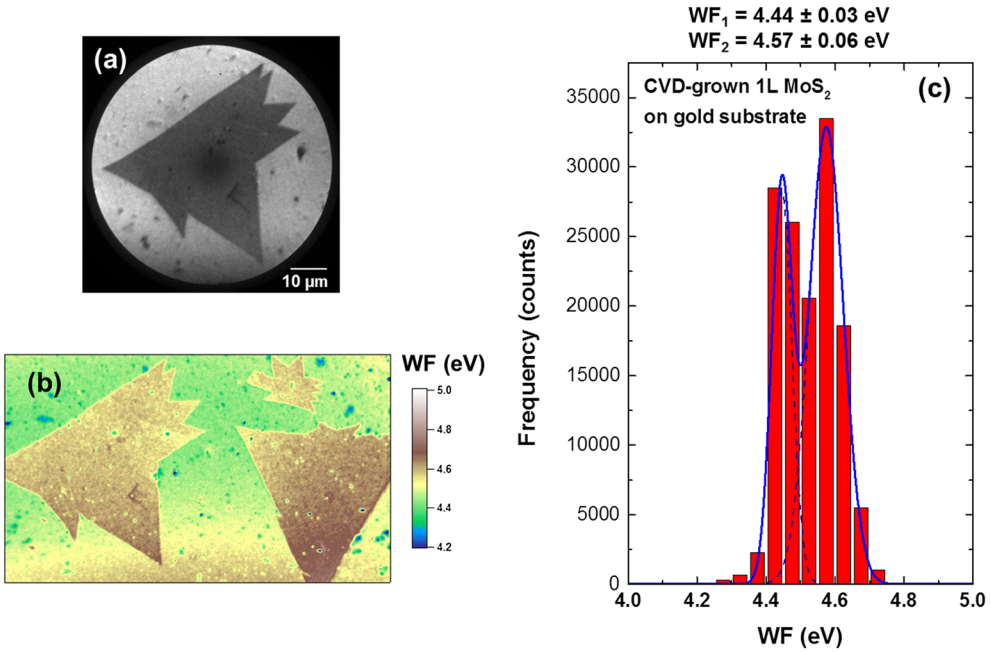

Figure 1. (a) Energy filtered PEEM image ($E\text{–}E_F = 4.5$ eV, field of view of 67 μm) of a MoS_2 1L domain transferred onto Au substrate. (b) Corresponding work-function map within a field of view of 115 μm and (c) WF distribution histogram.

function value that was used to generate the work function map [6,13]. The typical lateral resolution and sensitivity of the measurement were between 50–150 nm and 20 meV, respectively. By fitting the work-function distribution extracted from the histogram (Fig. 1 (c)), two work function values were obtained. The lowest value, WF_1, at 4.44 ± 0.03 eV can be assigned to the substrate contribution. This is certainly a low work function value for a gold surface, but it may be because of its deposition process or a possible interdiffusion of species between the underlying silicon wafer and the gold film [14]. Concerning the second contribution, WF_2 at 4.57 ± 0.06 eV, it can be attributed to the MoS_2 domain, because this value is very close to the one obtained on bulk single-crystal MoS_2 (4.55 ± 0.1 eV) [15]. Overall, the map highlights a uniform work-function over both domains imaged within the field of view. Because the work function value is extremely surface sensitive, one can conclude that both surface chemistry and electronic properties are the same all over a particular domain.

Figure 2 (a) shows an energy-filtered XPEEM image of a CVD MoS_2 1L domain transferred onto a Si substrate. The high contrast in PEEM and more specifically the rather uniform work-function value measured within the domain (Fig. 1) revealed that the latter was composed of a high-quality MoS_2 1L crystal, which will make it suitable for *k*PEEM measurements (see below).

XPS micro-spectroscopy was used to investigate the surface chemical states and relative elemental concentration of the 1L MoS_2 domain imaged by energy-filtered XPEEM at threshold (secondary electrons) in Fig. 2 (a). Figure 2 (b) exhibits the corresponding XPS survey micro-spectrum obtained. It clearly evidences the presence of molybdenum (Mo) and sulfur (S) in the CVD-grown area. In addition to these two elements, an intense contribution of Si and oxygen (O) is detected originating from the underlying Si oxide substrate and underlines, at the same time, the atomically thin character of the MoS_2 sheet. This was further confirmed directly by the core-level spectroscopic imaging of Mo, S and Si. The residual presence of carbon may be because of the CVD growth conditions. This has no significant influence on the quality of the surface because the measured work function, as shown previously, is consistent with bulk MoS_2.

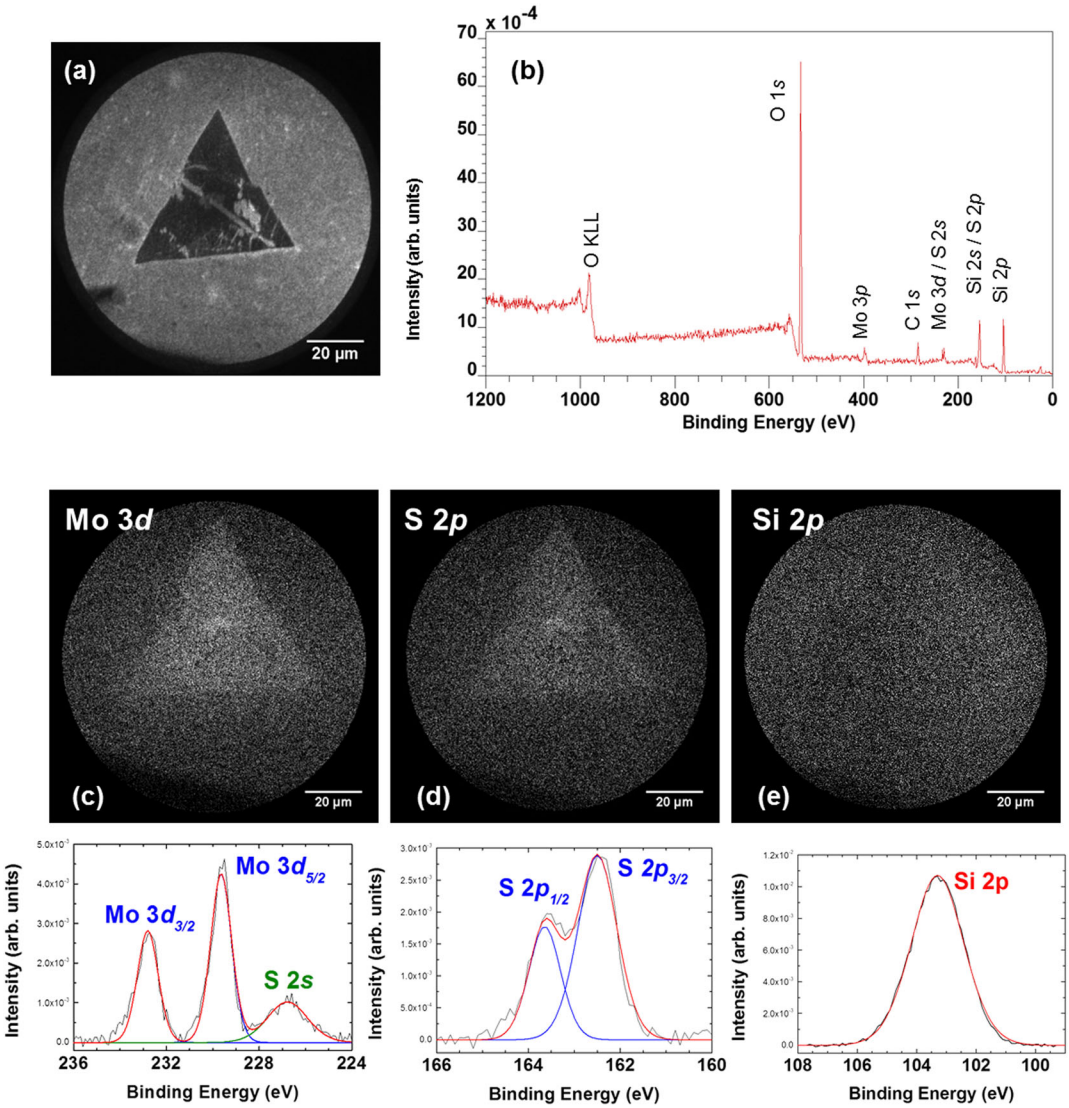

Figure 2. (a) Energy filtered PEEM image (threshold, $E–E_F = 3.3$ eV) of a MoS_2 1L domain transferred onto Si substrate and (b) corresponding XPS survey micro-spectrum. Integrated Mo 3d (BE ~ 230 eV) (c), S 2p (BE ~ 163 eV) (d), Si 2p (BE ~ 103 eV) (e) core level peak area image of the identical region as the one shown in (a). The corresponding high-resolution spectra with component peak fitting are presented at the bottom. The peaks were fitted using the asymmetric/symmetric Voigt functions using CASA XPS software.

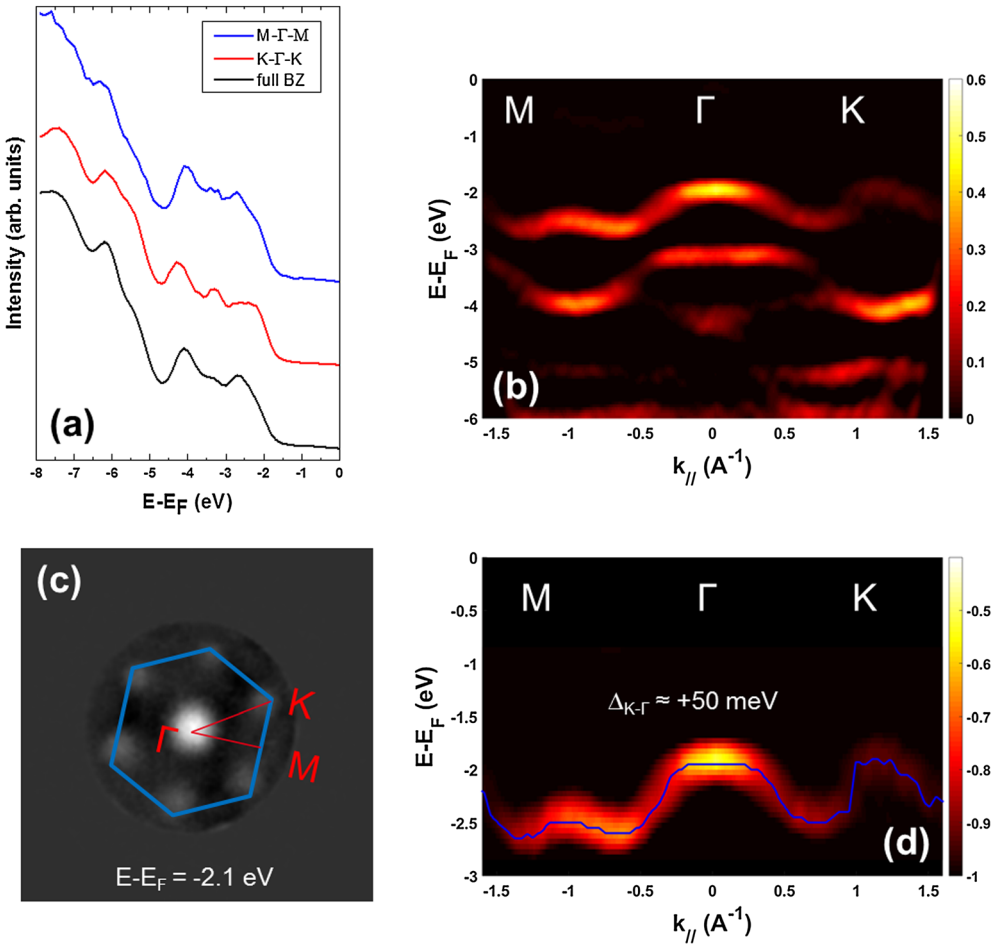

Figure 3. (a) Angle-integrated valence band spectra of CVD-grown MoS_2 1L on SiO_2/Si extracted along the high-symmetry directions ($\overline{M}$-$\overline{\Gamma}$-$\overline{M}$) and ($\overline{K}$-$\overline{\Gamma}$-$\overline{K}$) of the BZ and over the full BZ. (b) Energy filtered kPEEM image ($E-E_F = 16.9$ eV) showing the high-symmetry points of the hexagonal BZ. (c) Measured band dispersions of CVD-grown MoS_2 1L along the $\overline{M}$-$\overline{\Gamma}$-$\overline{K}$ high-symmetry directions of the BZ and (d) zoom in the upper valence band (UVB) region; the blue curve represents the maximum intensity of the UVB.

The Mo 3*d* and S 2*p* core level integrated area images on Fig. 2 (c) and (d) show that there is a clear contrast between the CVD material and the Si substrate region. This correlates well with the work-function mapping of the MoS_2 domain on Au substrate presented in Fig. 1. Moreover, insights on the MoS_2 surface composition can be obtained from the high-resolution Mo 3*d* and S 2*p* core-level spectra of the 1L MoS_2 retrieved from the spectroscopic image series of the area, as shown in spectra of Fig. 2 (c) and (d) after Shirley background and peak fitting. The Mo 3*d* spectrum consists of peaks at 229.6 and 232.8 eV that correspond to Mo^{4+} $3d_{5/2}$ and Mo^{4+} $3d_{3/2}$ components of MoS_2, respectively. No metallic Mo is found to lower binding energy. It is also worth noting that no peak at around 236 eV, which corresponds to Mo^{6+} $3d_{5/2}$, is detected: this indicates that oxidation of Mo is absent or very weak. In the S 2*p* spectrum we find the well-known doublet peaks of MoS_2, S $2p_{1/2}$ and S $2p_{3/2}$, which appear at 163.6 and 162.5 eV, respectively. Similarly, no peaks were observed between 168 and 170 eV, which indicates that sulfur atoms also remain non-oxidized.

The relative surface concentrations of the MoS_2 domain were determined from the measured integrated areas. The corresponding sensitivity factor was derived from the photoionization cross section, and we assumed similar transmission of Mo 3*d* and S 2*p* photoelectrons. Thus, the atomic concentration was found to be 37.6 and 62.4% for Mo and S, respectively. Despite a small excess of Mo, possibly because of a rather simplified quantification procedure, this is fairly consistent with a 2:1 sulfur stoichiometry. Finally, the Si 2*p* core level image of Fig. 2(e) shows virtually no contrast, evidencing a negligible attenuation of the photoemission signal from Si through the MoS_2 domain, thus confirming its ultra-thin character. However, because the escape depth of Si 2*p* photoelectrons in our measurement condition is 2.96 nm (i.e. the inelastic mean-free path with Al Kα excitation), the probing depth is already greater than the thickness measured by AFM and expected for 1L-thick MoS_2.

Finally, we present the *k*PEEM measurements performed on MoS_2 1L transferred onto Si substrate. The measured valence band of MoS_2 is derived from hybridization of the Mo *4d* and S *3p* orbitals [1,16]. Figure 3 (a) shows angle-integrated photoemission spectra of CVD-grown MoS_2 1L extracted from high-symmetry directions ($\overline{M}$-$\overline{\Gamma}$-$\overline{M}$), ($\overline{K}$-$\overline{\Gamma}$-$\overline{K}$) and over the full BZ (see Fig. 3 (c)). Because of an overall energy shift in the final, summed-up series because of residual charging, these spectra were energy-rescaled to match the same energy range as 1L MoS_2 transferred onto Au substrate. The angle-integrated (full Brillouin zone) valence-band spectrum of Fig. 3(a) shows an onset feature approximately 1.70 eV below the Fermi level. Because 1L MoS_2 band gap is ~1.90 eV [17,18], besides providing support to our calibration procedure (which does not seem to introduce unreasonable, large errors) this would indicate

that CVD grown-MoS_2 is electron-doped which is consistent with previous papers [16,19]. The higher onset energy compared to Ref. 17 however, suggests a larger *n*-doping level, likely because of the different processing conditions (exfoliated MoS_2 in Ref.17 vs CVD-grown material in our case). Figure 3 (b) presents the measured band dispersions of CVD-grown MoS_2 1L along the $\overline{M}\overline{\Gamma}\overline{M}$ high-symmetry directions of the BZ. The obtained band structure is in rather good agreement with previous DFT band calculations taken into account spin–orbit interaction [3]. Indeed, the ARUPS band map exhibits three specific features of the valence band including maxima at $\overline{\Gamma}$ and $\overline{M}$ originating from Mo d_z [2] (out-of-plane orbitals) and another one at $\overline{K}$ induced by Mo d^2_{xy} /d_{xy} (in-plane orbitals) [20]. As expected from our analysis geometry (grazing illumination), the VBM at $\overline{\Gamma}$ is very intense and the band curvature is well-defined unlike previously published work [16] using normal-incidence photon excitation.

Figure 3 (d) focuses on the valence band map in the upper valence band (UVB) region. Although our energy resolution does not allow us to resolve the spin–orbit splitting near $\overline{K}$, we can claim that the VBM is located at $\overline{K}$ instead of $\overline{\Gamma}$, based on the assessment of the UVB energies determined at $\overline{K}$ and $\overline{\Gamma}$ from the intensity maxima at the corresponding point in the k-space (blue curve). DFT calculation predicts an energy separation of the VBM at $\overline{K}$ and $\overline{\Gamma}$ of ~100 meV[3] which is quite close to our experimental value $\Delta_{K-\Gamma} = \mathrm{UVB}(\overline{K}) - \mathrm{UVB}(\overline{\Gamma})$ of 50 meV. Here, because we deal with the maximum of a peak in the UVB rather than peak separation, sensitivity matters more than energy resolution, in such a way that the derived $\Delta_{K-\Gamma}$ value is representative of an intrinsic electronic property of the MoS_2 domain. Indeed, this feature of the UVB at $\overline{K}$ is specific of MoS_2 1L because for few-layer or bulk MoS_2, the VBM at $\overline{K}$ is lower than at $\overline{\Gamma}$ due the indirect band gap. The result from our *k*PEEM data correlates well with the pronounced peak at ~1.8–1.9 eV detected in photoluminescence (spectrum not shown here) and tends to demonstrate that the CVD grown material is effectively 1L MoS_2 with reasonable good structural integrity. This small difference provides support for the direct band gap transition in 1L MoS_2, as seen in photoluminescence studies [2,17]. This change in electronic structure is generally attributed to quantum confinement [2,18].

Finally, hole effective masses of CVD-grown MoS_2 1L could be extracted from our *k*PEEM measurements. Indeed, simple parabolic fits of the UVB at $\overline{\Gamma}$ and $\overline{K}$ allowed us to experimentally determine the hole effective masses of $(2.07 \pm 0.04)\ m_0$ and $(0.66 \pm 0.04)\ m_0$, respectively. The latter are in good agreement with those obtained on exfoliated MoS_2 1L: $(2.00 \pm 0.35)\ m_0$ and $(0.43 \pm 0.02)\ m_0$, respectively [21]. These rather high values of effective mass at $\overline{\Gamma}$ in MoS_2 1L are known to be responsible of the relatively poor carrier mobility ($<10\ cm^2/V.s$) [19] of MoS_2 1L compared with its bulk counterpart (50–200 cm^2/V.s at room temperature).

In summary, a comprehensive set of photoelectron spectroscopic techniques by XPEEM using laboratory excitation sources was applied to CVD-grown MoS_2 1L micro-domains. The measurements provide important information, ranging from work function and surface chemical states to electronic band structure. Core level chemical analysis and surface work function mapping revealed high-quality triangular CVD 1L MoS_2 domains with a grain size of few ten micrometers. *k*PEEM measurements were performed to probe the valence bands of this single-layer MoS_2. The results reveal a rather good qualitative and quantitative agreement with previous data on exfoliated samples and theoretical predictions, such as VBM at $\overline{K}$ instead of $\overline{\Gamma}$ and hole effective mass values. The easy-accessible and consistent measurements reported here help to qualify effectively 2D-MoS_2 and other related materials, without the need of synchrotron radiation.

Acknowledgements

This work was performed at the Nanocharacterization Platform (PFNC) of MINATEC Campus, CEA-Grenoble. MF acknowledges the Nanoscience/Chimtronique 2015 Program of CEA within the CASCADE project for funding.

References

[1] L. F. Mattheiss, *Physical Review B* **1973**, *8*(8), 3719.
[2] A. Splendiani, S. Liang, Y. Zhang, T. Li, J. Kim, C.-Y. Chim, G. Galli, F. Wang, *Nano Lett* **2010**, *10*(4), 1271.
[3] Z. Y. Zhu, Y. C. Cheng, U. Schwingenschlögl, *Physical Review B* **2011**, *84* (15), 153402.
[4] B. Radisavljevic, A. Radenovic, J. Brivio, V. Giacometti, A. Kis, *Nat Nano* **2011**, *6*(3), 147.
[5] M. Escher, N. Weber, M. Merkel, C. Ziethen, P. Bernhard, G. Schönhense, S. Schmidt, F. Forster, F. Reinert, B. Krömker, D. Funnemann, *J Phys Condens Matter* **2005**, *17*(16), S1329.
[6] M. Escher, K. Winkler, O. Renault, N. Barrett, *Journal of Electron Spectroscopy and Related Phenomena* **2010**, *178–179*, 303.
[7] O. Renault, *Surf Interface Anal* **2010**, *42*(6–7), 816.
[8] a H. K. Kim, O. Renault, A. Tyurnina, J.-P. Simonato, D. Rouchon, D. Mariolle, N. Chevalier, J. Dijon, *Appl Phys Lett* **2014**, *105*(1), 011605; b C. Mathieu, O. Renault, H. Rotella, N. Barrett, A. Chabli, *AIP Conference Proceedings* **2011**, *1395*(1), 95.
[9] aO. Renault, M. Lavayssière, A. Bailly, D. Mariolle, N. Barrett, *Journal of Electron Spectroscopy and Related Phenomena*, (**2009**) *171* (1–3), 68; b N. Barrett, L. F. Zagonel, O. Renault, A. Bailly, *J Phys Condens Matter* **2009**, *21*(31), 314015.
[10] O. Renault, A. Garnier, J. Morin, N. Gambacorti, F. Bertin, *Appl Surf Sci* **2012**, *258*(24), 10077.
[11] R. Kappera, D. Voiry, S. E. Yalcin, W. Jen, M. Acerce, S. Torrel, B. Branch, S. Lei, W. Chen, S. Najmaei, J. Lou, P. M. Ajayan, G. Gupta, A. D. Mohite, M. Chhowalla, *APL Materials* **2014**, *2*(9), 092516.
[12] H. Li, Q. Zhang, C. C. R. Yap, B. K. Tay, T. H. Tong Edwin, A. Olivier, D. Baillargeat, *Adv Funct Mater* **2012**, *22*(7), 1385.
[13] O. Renault, R. Brochier, A. Roule, P. H. Haumesser, B. Krömker, D. Funnemann, *Surf Interface Anal* **2006**, *38*(4), 375.
[14] A. Bailly, O. Renault, N. Barrett, L. F. Zagonel, P. Gentile, N. Pauc, F. Dhalluin, T. Baron, A. Chabli, J. C. Cezar, N. B. Brookes, *Nano Lett* **2008**, *8*(11), 3709.
[15] R. H. Williams, A. J. McEvoy, *physica status solidi* **1971**, *47*(1), 217.
[16] W. Jin, P.-C. Yeh, N. Zaki, D. Zhang, J. T. Sadowski, A. Al-Mahboob, A. M. van der Zande, D. A. Chenet, J. I. Dadap, I. P. Herman, P. Sutter, J. Hone, R. M. Osgood, *Physical Review Letters* **2013**, *111*(10), 106801.
[17] K. F. Mak, C. Lee, J. Hone, J. Shan, T. F. Heinz, *Phys Rev Lett* **2010**, *105*(13), 136805.
[18] A. Kuc, N. Zibouche, T. Heine, *Physical Review B* **2011**, *83*(24), 245213.
[19] K. S. Novoselov, D. Jiang, F. Schedin, T. J. Booth, V. V. Khotkevich, S. V. Morozov, A. K. Geim, *Proc Natl Acad Sci U S A* **2005**, *102*(30), 10451.
[20] a S. W. Han, G.-B. Cha, E. Frantzeskakis, I. Razado-Colambo, J. Avila, Y. S. Park, D. Kim, J. Hwang, J. S. Kang, S. Ryu, W. S. Yun, S. C. Hong, M. C. Asensio, *Physical Review B* **2012**, *86*(11), 115105; b E. Cappelluti, R. Roldán, J. A. Silva-Guillén, P. Ordejón, F. Guinea, *Physical Review B* **2013**, *88*(7), 075409.
[21] W. Jin, P.-C. Yeh, N. Zaki, D. Zhang, J. T. Liou, J. T. Sadowski, A. Barinov, M. Yablonskikh, J. I. Dadap, P. Sutter, I. P. Herman, R. M. Osgood, *Physical Review B* **2015**, *91*(12), 121409.